Dynamic Operation of a Storage Power Plant (SPP) with Voltage Angle Control as Ancillary Service

Paul Gerdun, Nayeemuddin Ahmed, Vinaykumar Vernekar, Martin Töpfer, Harald Weber
Electrical Energy Supply (EEV), Institute for Electrical Power Engineering (IEE)
University of Rostock
Rostock, Germany
{paul.gerdun, nayeemuddin.ahmed, vinaykumar.vernekar, martin.toepfer, harald.weber}@uni-rostock.de

***Abstract*—It is expected that in the near future, the electrical power supply networks will be significantly revolutionized. Today's conventional power plant structures will give way to a novel, inertia independent (free from rotating masses) power plant system. Such power stations, called storage power plants, will possess storages for different generation speed together with power electronic converters. They will be able to integrate and store energy from renewable sources. Since such a system will not possess any flywheels or rotating masses, thus frequency control as utilized in conventional power plants will be redundant. All the control principles necessary involving spinning reserve, primary and secondary control depending on frequency will be substituted by a comprehensive angle control of the nodal voltages in the transmission and distribution network. However, to be deemed truly feasible, these storage power plants must be able to function efficiently when they are integrated with conventional power plants and renewable energy sources. Thus, in this paper, these power plants are connected with conventional thermal and hydroelectric power stations as well as wind power plants, in a single network, and their dynamic behavior is studied under nodal voltage angle control as the ancillary service.**

***Index Terms*—ancillary, inertia, nodal voltage angle, primary control, secondary control, spinning reserve, storage**

I. Introduction

Currently, 14.8% of Germany's gross final energy consumption (approximately 2500 TWh) originates from renewable energy sources (RES) [1]. The aim of the EU 2020 energy strategy is to raise this share to 18% with future targets projecting it to be around 60% by the year 2050 [2]–[5]. Such high penetration of renewable energy (wind and solar), although necessary, introduces additional challenges in ensuring stability and reliability of the electrical grid. The ever increasing feed in from these RES leads to higher frequency fluctuations, presence of harmonics as well as increased forecast errors due to their intermittent nature [6].

The difference between the varying electrical energy generation from RES and consumption by loads leads to an energy deficit or surplus in the grid. At present, conventional power plants (CPP) have to compensate for this disparity. However, in the future, the number of these CPP, especially coal fired power plants, will decrease significantly to fulfill energy sector targets [7]. Thus, Electrical Energy Storage (EES) systems are regarded as viable alternatives to compensate for the intermittent and decentralized RES, so that the network demand can be met at all times [8].

Depending on its principle a storage type has different advantages and disadvantages. Flywheels and Supercapacitors have high charge and discharge rates, but, due to their sizes, are impractical long-term energy storages [9]. In comparison to supercapacitors, battery energy storages have a higher energy density but a much slower response [10]. Hydrogen storages can be used to store large magnitudes of energy but due to the electrochemical reactions via a fuel cell or electrolyser their response is even slower. A combination of these elements, though, will not only compensate for the shortcomings of these individual storage types but also assist in exploiting their advantages. Hence, such an interconnected system is presented in this paper, called Storage Power Plant (SPP).

In the future, with most of the traditional power plants (possessing rotating masses) being replaced by an increasing number of converters in the grid, a frequency independent governing principle can be used. Such a form of ancillary service is called Voltage Angle Control [11]–[13]. The SPP to be deemed truly feasible has to function efficiently with CPP in both present and future day scenarios. Thus, the goal of this paper is to show the coherent operation of CPP and SPP in a nodal voltage angle controlled grid.

II. Investigated Network Structure

The example network on which the investigations are carried out is shown in Fig. 1. The grid consists of 25 equidistant nodes, each connected to either a power plant or a load. The nodes are interconnected via transmission lines, each 250 km long and at a voltage level of 110 kV. The line impedances are equal in magnitude with a resistance to reactance ratio of 0.1. Such a squared grid is used to easily highlight the power production principles when the electrical network is governed by nodal voltage angle control. This will become more apparent once Fig. 3 is analyzed.

There are eleven power plants, of which five are slack SPPs (S), i.e. converters at terminals where the voltage magnitude ($|V|$) and angle (ϕ_u) are kept constant. Out of the other six power plants, four represent wind power plants (W), while the other two each represent a conventional hydroelectric (H) and thermal (T) power plant. At these PV terminals, the active power (P) and voltage magnitude ($|V|$) are controlled. The remaining 14 nodes are each connected to a PQ consumer i.e.

978-1-7281-1156-8/19/$31.00

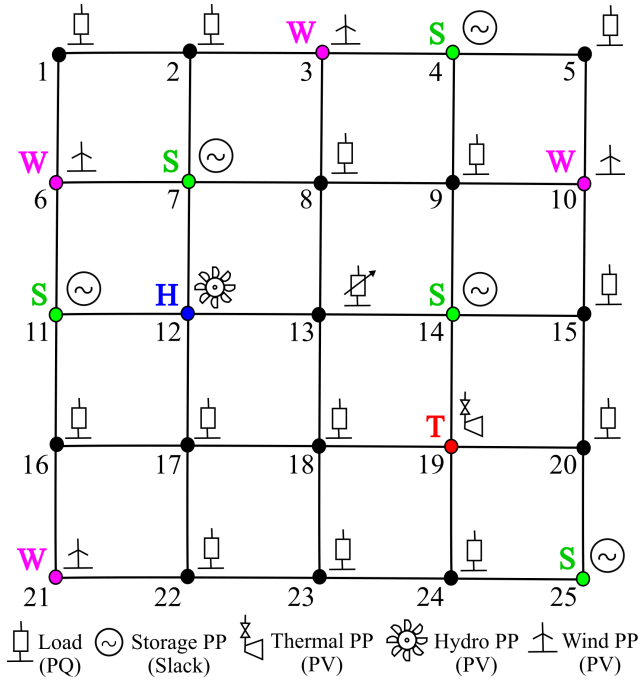

Fig. 1. 25 node example network

loads at terminals where the active (P) and reactive power (Q) being consumed are known.

The network modeling and simulations are carried out in the software DIgSILENT PowerFactory. The base power value of the per-unit-system is 10 MVA. It is assumed that each of the 14 loads consumes 10 MW of active power. The total deficit of 140 MW is equally satisfied by the two conventional and four wind power plants, each producing almost 23.3 MW to meet this demand. The SPPs are initially kept at a working point of 0 MW. Thus, a positive power output would correspond to SPPs supplying power, while a negative value would mean that they are storing power as per the network requirement.

Each load also consumes 3.33 MVAR of reactive power which is supplied later by the power plants. Unfortunately, the reactive power results and control methods are not included in this paper due to space constraints. However, it can be mentioned that the system has an improved relation between reactive power and voltage (Q-V characteristic) under the voltage angle control method due to the voltage stabilizing ability of the slacks.

III. Internal SPP Structure

As seen in Fig. 2, the SPP consists of three main storages, namely the supercapacitor, battery and hydrogen storage. These storages have different energy capacities and are responsible for providing either inertial, primary or secondary control. There are DC-DC converters positioned between the storages which control the power flow between them. All components operate in DC mode. Therefore, the power plant uses a DC-AC converter for grid connection. The SPP structure used in the software, models the control scheme of the DC-DC converters which govern the power flow between the SPP storage components. The components themselves are represented by simplified ideal models.

The first storage, i.e. the supercapacitor, is directly connected to the DC-AC grid converter. In case of a network disturbance, it immediately supplies inertial power to the grid or stores it from the grid. It can instantaneously charge and discharge with high power and additionally has an almost infinite lifetime because of its electrostatic storage principal. This makes it the ideal type of storage for its task of providing inertial control. Hence, its behavior is analogous to the rotating mass in a turbine shaft of a conventional thermal power plant.

The second storage, i.e. the battery, connected in parallel to the supercapacitor, supplies or stores primary control power, in order to compensate for the low power density of the supercapacitor. This process is controlled by the DC-DC

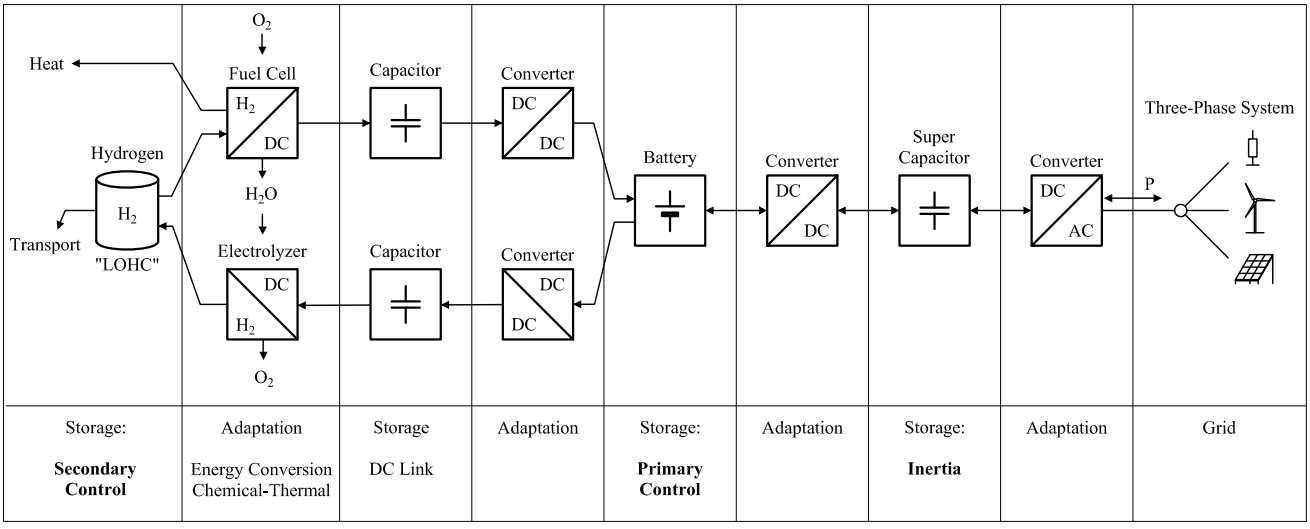

Fig. 2. Working principle of the internal components of a storage power plant (SPP)

converter between these two components. In contrast to a supercapacitor, the battery is optimally suited for the purpose to provide primary control power because of its electrochemical energy storage principle which allows it to possess a higher energy storage density and a preferably lower charging and discharging gradient, to improve its lifetime. Thereby, it represents the equivalent of the steam boiler in a conventional thermal power plant.

As the third main storage, the hydrogen storage is responsible for supplying secondary control power, like coal in a conventional thermal power plant. Additionally, it can store secondary control power. Depending on the power flow direction, either a fuel cell or an electrolyser is used to empty or refill the hydrogen storage. The power flow for each of these directions is controlled by the DC-DC converter in the respective paths between the hydrogen storage and the battery. Each of these two DC-DC converters possess a DC link buffer storage whose behavior is analogous to the steam boiler pipe wall in a conventional thermal power plant.

While utilizing the hydrogen storage, the fuel cell generates electrical energy by the chemical reaction between stored hydrogen (H_2) and external oxygen (O_2). One byproduct of this reaction is thermal energy which can be used for district heating. Another product is dihydrogen monoxide (H_2O). In case of a reversed power flow, the H_2O can in turn be used as the electrolyte to generate hydrogen as well as oxygen as a byproduct. The hydrogen can then be stored in a Liquid Organic Hydrogen Carrier (LOHC) system. Such a system enables safe, easy storage and transportation of hydrogen at a high energy density under ambient conditions, using the currently available infrastructure [14]. In addition to being used for electrical power generation in the SPP, the stored hydrogen can also be utilized for other applications, for example in automobiles.

IV. Study Case

To analyze the dynamic behavior of the SPPs, a sample case study is performed by applying a step increase followed by a step decrease to the active power demand in the load at node 13 of the network. This causes the power consumption at this node to increase after 20 s from 10 MW to 17 MW and then decrease after 300 s to 3 MW. The magnitude of the step increase and decrease corresponds to 5% and -10% of the total power consumption (140 MW) in the network.

In response, the steady state frequency does not change, since the grid is governed by nodal voltage angle control. Therefore, the CPP at nodes 12 and 19 as well as the wind turbines at nodes 3, 6, 10 and 21, which are governed by a typical frequency controlled structure, act as PV nodes and keep their power output constant.

As seen in Fig. 3, the increase in the active power output of each SPP in response to the load change depends directly on its electrical proximity to the changed load. The SPP at node 14 is located right next to the changed load, i.e. load at node 13. Therefore, this SPP supplies the highest amount of power when compared to the other SPPs. The lowest increase

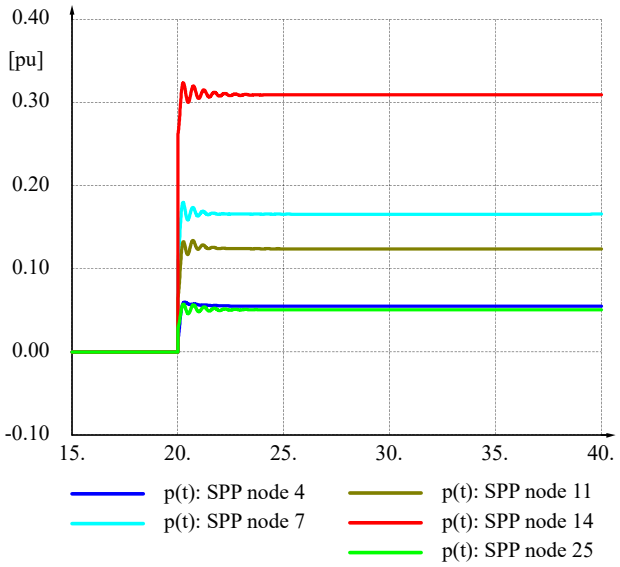

Fig. 3. Increase in active power generation of all the SPPs in response to the initial step increase in load demand at node 13

in power output is exhibited by the SPP at node 25 since it is also the farthest SPP from the changed central load. Due to the resistance in the transmission lines, there will be some losses during the power flow and the total additional power supplied by the SPPs will be greater than the power demand increase of the load at node 13.

In a network governed by nodal voltage angle control, the ancillary services are load flow oriented and are provided by the angle controlled power plants close to the point of disturbance. As opposed to frequency control, this allows the power plants farther away to remain undisturbed. These trends are pronounced due to the use of a squared grid, as shown in Fig. 1. In a grid with a non-uniform distribution of the line impedances, it would not be as easy to highlight the principles of power production with such clarity with the SPPs being governed by voltage angle control.

Next, the behavior of the internal components of the SPP at node 14 is investigated to examine how the inertial, primary and secondary control power are provided as ancillary services due to these sudden disturbances in load power consumption.

V. Results and Observations

Fig. 4a shows the active power output of the SPP at node 14. Fig. 4b illustrates the currents out of the respective storages while Fig. 4c exhibits the resulting change in the voltage or mass levels of these three storages. These trends are presented in three different time scales in Fig. 4-6, in order to highlight the ancillary services provided by the SPP and the storages associated with each of the control powers.

A. SPP Short Time Frame Response

The graphs in Fig. 4 show that, like rotating masses, the supercapacitor immediately starts to supply inertial power with the onset of the positive disturbance, so the SPP can meet

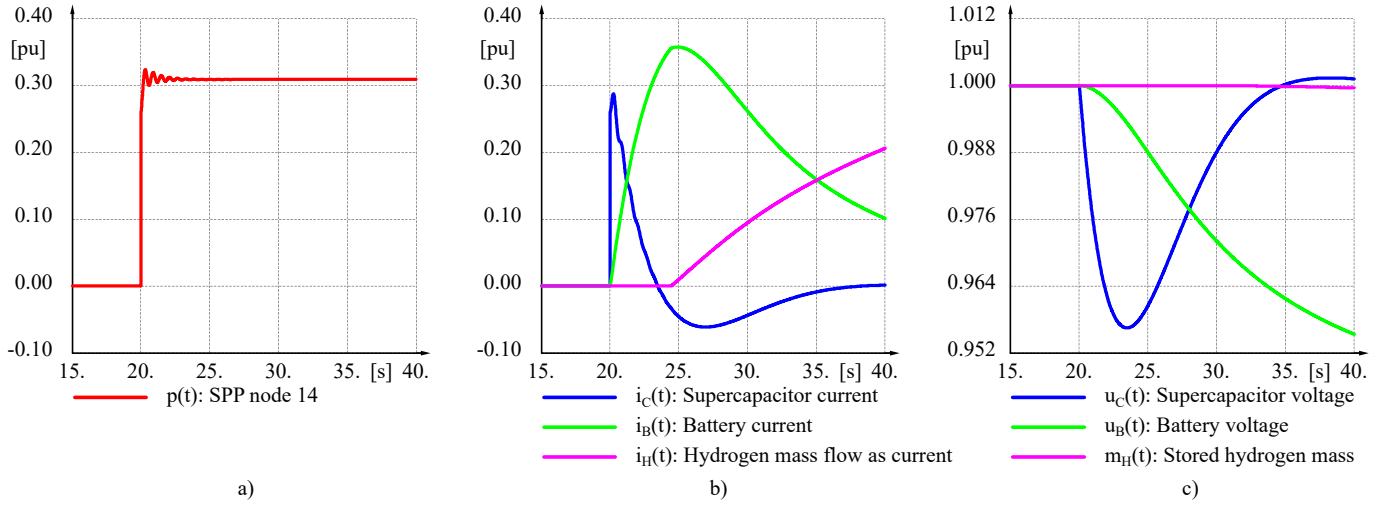

Fig. 4. a) Increase in power output, b) Current flow from the SPP storages and c) Voltage levels of the storages during the initial short time frame

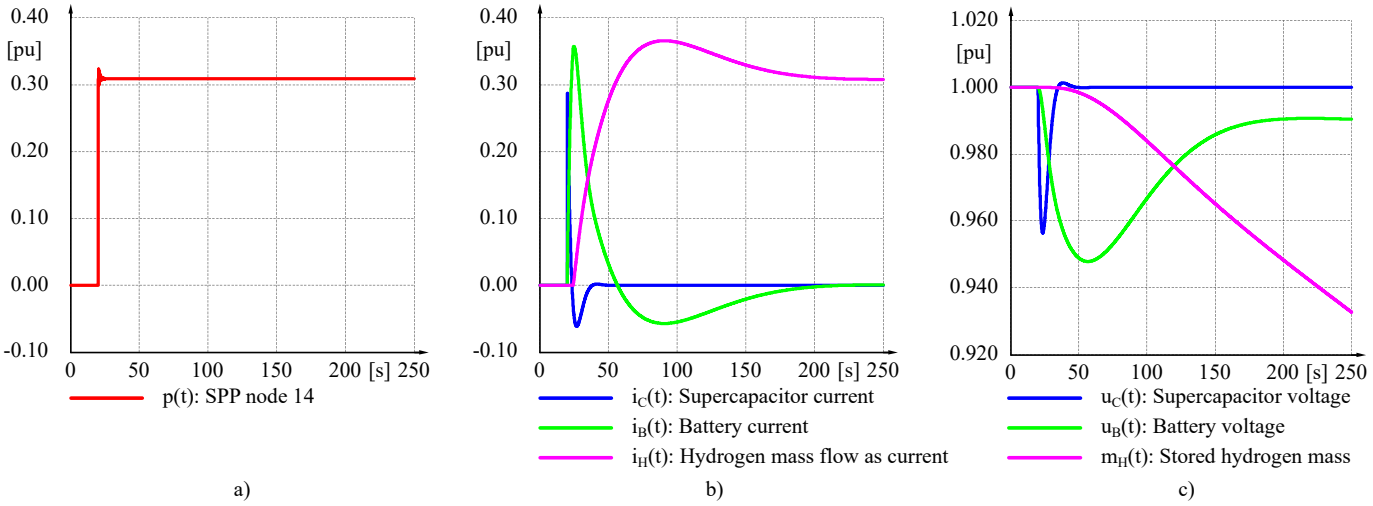

Fig. 5. a) Increase in power output, b) Current flow from the SPP storages and c) Voltage levels of the storages during the medium time frame

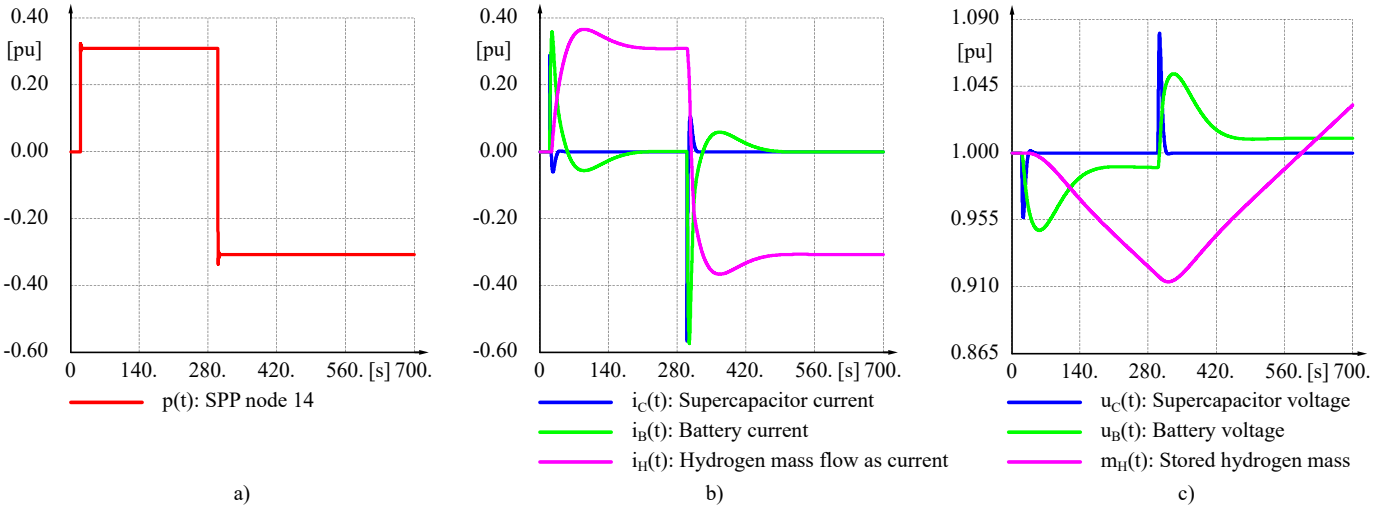

Fig. 6. a) Increase in power output, b) Current flow from the SPP storages and c) Voltage levels of the storages during the long time frame

the increased network demand. As a result, the supercapacitor voltage decreases. To ensure that the supercapacitor is able to respond to further disturbances, the DC-DC converter between the supercapacitor and battery takes over supplying the disturbed network demand and subsequently recharges the supercapacitor to its nominal value. The recharging phase of the supercapacitor is visible in Fig. 4b for the time duration when the supercapacitor current is negative.

B. SPP Medium Time Frame Response

For this primary control, the DC-DC converter uses only the energy stored in the battery. Therefore, the battery current increases and its voltage decreases. In addition, the DC-DC converter limits the battery current gradient to lower the stress on the storage device and in the process improves its lifetime.

The battery voltage operates within a defined voltage dead band under steady state conditions. When the battery voltage surpasses the lower threshold of 0.99 pu in Fig. 5c, the DC-DC converter on the upper branch between the battery and the fuel cell in Fig. 2, increases its power flow to the grid. This continues until it fully supplies the disturbed network demand on its own. Furthermore, the converter recharges the battery and raises its voltage to be within permissible limits of the dead band. It is able to perform these functions since it controls its adjacent fuel cell. As a result, it increases the power supplied from the fuel cell, according to the required power demand of the grid. This supply of secondary control power can be seen in the form of increased hydrogen mass flow in Fig. 5b.

C. SPP Long Time Frame Response

In the first half of the longer time frame represented in Fig. 6c, the consequent decrease in the stored hydrogen mass is shown. During steady state operation the network demand is fully supplied by the hydrogen storage alone. However, the SPP is not only able to supply power to the grid, like a CPP, but can also store it. This is depicted in the SPP response to a negative load change, i.e. load reduction at node 13, shown in the second half of Fig. 6a. The change leads to an active power surplus in the grid.

The supercapacitor and battery behave similarly to the positive load jump, but the changes are in the opposite direction due to the reversed power flow in response to this disturbance. In this case, when the battery voltage crosses its upper dead band threshold of 1.01 pu, the DC-DC converter between the battery and the electrolyser gradually increases its power flow to the hydrogen storage. This continues till the surplus disturbed network power is transferred entirely to the hydrogen storage. Subsequently the converter discharges the battery until its voltage is within the dead band again. As seen in the second half of Fig. 6c, the stored hydrogen mass increases as a result.

D. Output comparison between the SPPs at nodes 7 and 14

Fig. 7a exhibits the isolated changes in the power output of the SPPs at nodes 7 and 14, as a result of the initial step increase in the load power consumption at node 13 from 10 MW to 17 MW at 20 s. According to the principles of nodal voltage angle control, as discussed earlier in Fig. 3, the increase in the output of the SPP at node 14 is higher than the one at node 7 since the former is at a closer electrical proximity to the changing load at node 13.

The resulting changes in the capacitor, battery and hydrogen current flows inside the two SPPs are compared in Fig. 7b, signifying the ancillary services provided by each plant. Since the power output of the SPP at node 14 is higher, its peak capacitor, battery and hydrogen current, representing the maximum inertial, primary and secondary control power supplied, are also greater than the SPP at node 7. In addition, the rate of increase of the battery current for the SPP at node 7 is also lower than its counterpart. Due to this reduced gradient, the battery voltage of the SPP at node 7 crosses its lower threshold of 0.99 pu later than the one at node 14, as shown in Fig. 7c.

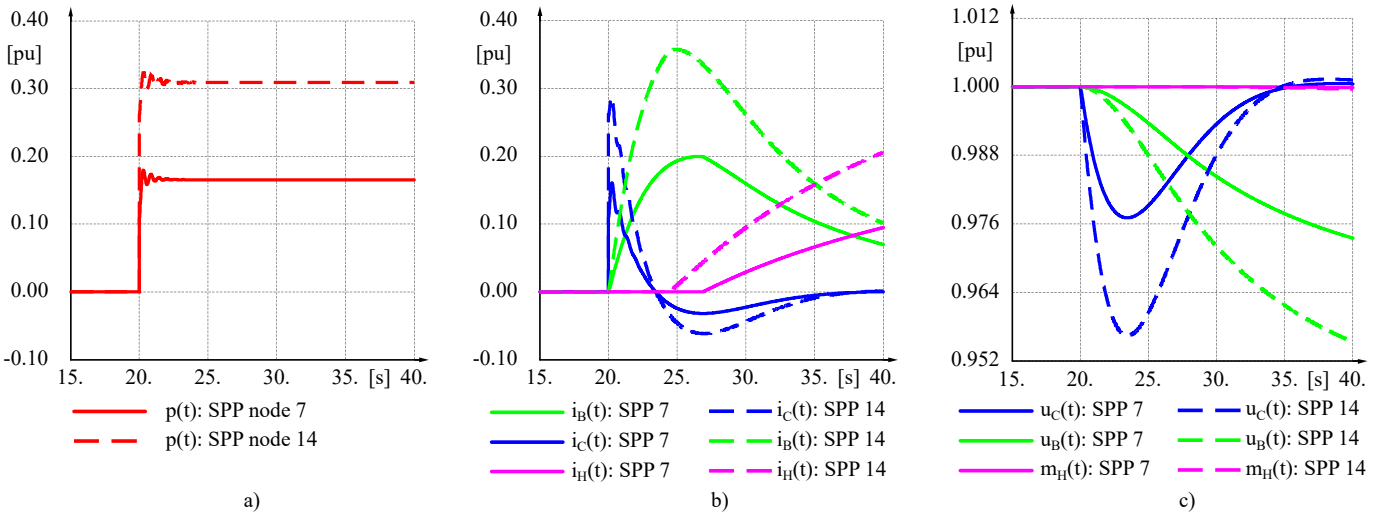

Fig. 7. a) Increase in power output, b) Current flow from the SPP storages and c) Voltage levels of the storages of the SPPs at node 7 and 14

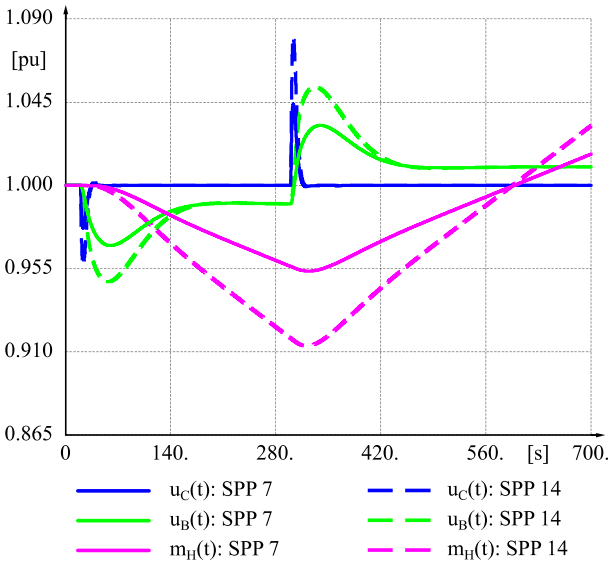

Fig. 8. Voltage levels of the storages of the SPPs at node 7 and 14 for a long time frame

This means that the hydrogen current, representing the mass flow rate of hydrogen from the fuel cell, starts to flow later for the SPP at node 7, as displayed in Fig. 7b.

Consequently, its hydrogen storage also starts to be emptied later and at a slower rate than that of the SPP at node 14. A clearer depiction of the changing hydrogen mass levels in the respective hydrogen storages of the two SPPs is shown in Fig. 8. The higher magnitude of the hydrogen current for the SPP at node 14 corresponds to the lower mass level of its storage. If the hydrogen level falls below a minimum threshold, the SPP stops working. This causes a change in the voltage angle at the same node and the ones around it. The other SPPs autonomously adjust their power output according to the changed nodal voltage angle and compensate for the idle SPP. The figure additionally shows the voltage levels of the supercapacitor and the battery of these SPPs for a longer time frame. These results suggest that the trends in the current flow from the storages and the associated voltage levels of these storages are similar for all the SPPs. The main difference lies in the peak magnitudes of every quantity, which, due to the principles of voltage angle control, are higher for an SPP closer to the changing load and lower for one that is farther away.

VI. Conclusion

This paper exhibited the ability of SPPs to function effectively with CPPs in a nodal voltage angle controlled grid. Therefore, a 25 node network with multiple types of power plants was used as a test environment. Inside this network, a disturbance was created by changing the load power consumption at the central node of the network and the corresponding dynamic response of the SPPs was investigated. It was shown that while supplying or storing power as a result of the disturbance, a SPP is able to provide the necessary ancillary response in the form of inertial, primary and secondary control. These power flows inside the SPP are regulated by the respective DC-DC converters between these storages.

The features of nodal voltage angle control as the ancillary service in the electrical network were also discussed. To highlight this, the power output of two SPPs at different electrical distances from the disturbance was compared. Currently, studies involving the subtransient and transient behavior of SPPs during short circuit faults are underway. The reactive power control schemes of the SPPs are also being investigated. In addition, further research will be required to estimate the total losses as well as the market compatibility of this novel system and hence prepare a quantitative comparative study in relation to the current power system.

VII. Acknowledgment

This paper was made within the framework of the research project “Netz-Stabil” and financed by the European Social Fund (**ESF/14-BM-A55-0025/16**). It is part of the qualification program “Promotion of Young Scientists in Excellent Research Associations - Programme for Excellence in Research in Mecklenburg-Western Pomerania”.

References

[1] International Energy Agency. (2016) IEA World Energy Balances. [Online]. Available: https://www.iea.org/statistics?country=GERMANY&year=2016&category=Energy%20consumption&indicator=TFCbySource&mode=chart&dataTable=BALANCES

[2] H. Weber, T. Hamacher, and T. Haase, “Influence of wind energy on the power station park and the grid,” *IFAC Proceedings Volumes*, vol. 39, no. 7, pp. 59–64, 2006.

[3] European Commission Directorate-General for Energy. (2011) Energy 2020. [Online]. Available: https://ec.europa.eu/energy/sites/ener/files/documents/2011_energy2020_en_0.pdf

[4] VGB POWERTECH Facts and Figures, “Electricity Generation,” 2018.

[5] Energiewende, “The Energy of the Future, fifth energy transition monitoring report,” 2015.

[6] X. Liang, “Emerging power quality challenges due to integration of renewable energy sources,” *IEEE Transactions on Industry Applications*, vol. 53, no. 2, pp. 855–866, 2016.

[7] *Phasing out Coal in the German Energy Sector*. German Institute for Economic Research (DIW Berlin), 2019.

[8] H. Ibrahim, A. Ilinca, and J. Perron, “Energy storage systems — Characteristics and comparisons,” *Renewable and sustainable energy reviews*, vol. 12, no. 5, pp. 1221–1250, 2008.

[9] I. Hadjipaschalis, A. Poullikkas, and V. Efthimiou, “Overview of current and future energy storage technologies for electric power applications,” *Renewable and sustainable energy reviews*, vol. 13, no. 6-7, pp. 1513–1522, 2009.

[10] B. Dunn, H. Kamath, and J.-M. Tarascon, “Electrical energy storage for the grid: a battery of choices,” *Science*, vol. 334, no. 6058, pp. 928–935, 2011.

[11] H. Weber, N. Ahmed, and P. Baskar, “Nodal voltage angle control of power systems with renewable sources, storages and power electronic converters,” in *2018 International Conference on Smart Energy Systems and Technologies (SEST)*. IEEE, 2018, pp. 1–6.

[12] H. Weber, P. Baskar, and N. Ahmed, “Power system control with renewable sources, storages and power electronic converters,” in *2018 IEEE International Conference on Industrial Technology (ICIT)*. IEEE, 2018, pp. 1–7.

[13] H. Weber, N. Ahmed, and P. Baskar, “Power re-dispatch reduction with nodal voltage angle control in electrical energy supply systems,” *IFAC-PapersOnLine*, vol. 51, no. 28, pp. 576–581, 2018.

[14] D. Teichmann, W. Arlt, P. Wasserscheid, and R. Freymann, “A future energy supply based on liquid organic hydrogen carriers (LOHC),” *Energy & Environmental Science*, vol. 4, no. 8, pp. 2767–2773, 2011.